An innovative aluminization process for solid oxide cell interconnects: From the design to the processing and testing

Materials & Design 250 (2025) 113592

Contents lists available at ScienceDirect

Materials & Design

journal homepage: www.elsevier.com/locate/matdes

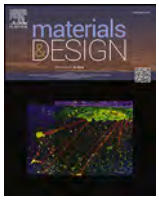

An innovative aluminization process for solid oxide cell interconnects: From the design to the processing and testing

E. Zanchi [a], H. Javed [b], S.De La Pierre [a], M. Ferraris [a], G. Cempura [c], A. Benelli [a,d], A.R. Boccaccini [e], F. Smeacetto [a,*]

[a] Department of Applied Science and Technology, Politecnico di Torino, Corso Duca degli Abruzzi 24 10129 Torino, Italy
[b] Sunfire GmbH, Gasanstaltstraße 2 01237 Dresden, Germany
[c] AGH University of Science and Technology, al. Mickiewicza 30 30-059 Krakow, Poland
[d] J-Tech@PoliTO, Turin 10129 Italy
[e] Department of Materials Science and Engineering, University of Erlangen-Nuremberg, Cauerstr. 6 91058 Erlangen, Germany

ARTICLE INFO

Keywords:
Solid oxide cells
Electrophoretic deposition
Joining

ABSTRACT

Applying an alumina-based coating at the sealant interface on interconnects can significantly reduce degradation and extend the lifetime of Solid Oxide Cell (SOC) stacks. This study introduces an innovative aluminization process achieved through Electrophoretic Deposition (EPD) of metallic aluminum powder on Crofer22APU stainless steel, reported here for the first time. The EPD suspensions and coating consolidation treatments were optimized for intermediate temperature applications in SOC stack interconnects. The alumina-based coating enhances steel resistance to high-temperature oxidation and improves the interface at the joined areas with the sealant by increasing surface roughness. Alumina-coated interconnect-glass sealant samples were subjected to static air ageing at 850 °C for up to 1000 h to evaluate interface evolution and potential corrosion product formation. The mechanical resistance of the alumina-coated steel joints, both in their initial state and after 1000-hour aging, was assessed via torsion tests, with a shear strength of 31.2 ± 2.0 MPa and 33.0 ± 1.0 MPa for as-prepared and aged samples, respectively, revealing a cohesive fracture mode and no interface degradation even after prolonged aging.

1. Introduction

The interconnect-sealant interface is critical for the durability of the Solid Oxide Cell (SOC) stack. Despite the efforts in the selection of both proper stainless-steel alloys for interconnects (ICs) and sealant compositions (e.g. a BaO-containing or SrO-containing silica-based glass), interface degradation phenomena are promoted by significant ions diffusion at SOC working conditions (i.e. high temperature, different polarisation between the metallic IC, ceramic spacers or electrolyte, dual atmosphere exposure). This leads to the possible formation of corrosion products and secondary phases, mainly identified as chromates (with a high coefficient of thermal expansion), causing the joint's mechanical resistance loss with a risk of delamination and gas leakage [1–7]. Therefore, the need for a protective coating between the IC and the sealant in SOC was first suggested in 2008 by Chou et al. [8], followed by a first study on the effect of the aluminization of FSS for SOC interconnects using as reference procedures the state-of-the-art aluminization process (e.g. commercial pack cementation, vapour phase deposition, aerosol spraying of aluminum salts) process based on aluminide coatings [9]. The deposition of the alumina-based coating was demonstrated to effectively reduce the formation of chromates.

The mentioned studies laid the groundwork for understanding critical issues arising from the deposition of aluminum-based coatings. Thereafter, a novel aluminization process specifically developed for SOC interconnects was proposed and named Reactive Air Aluminization (RAA) [10–12]. It is a multi-step process and involves the formulation of a slurry containing a mixture of organic binder/solvents and poor control of material usage. The RAA method consists of a slurry containing Al powder and a mixture of organic binder/solvents in a ratio of around 70:30 wt%. The slurry can then be applied by various deposition processes like screen printing, brush or spray painting, and dip coating; during the post-deposition consolidation aluminum partially oxidises in alumina and partially diffuses inside the steel substrate, resulting in a layer with enhanced surface roughness. In the RAA process, residual

* Corresponding author.
E-mail address: federico.smeacetto@polito.it (F. Smeacetto).

https://doi.org/10.1016/j.matdes.2025.113592
Received 8 October 2024; Received in revised form 23 December 2024; Accepted 5 January 2025
Available online 6 January 2025

alumina debris from unreacted coating should be removed in an ultrasonic bath before joining.

The final properties of the alumina coating strongly depend on the dimension of Al powder in the slurry and the thickness of the deposited layer and should be carefully balanced. Indeed, too small particles and/or thin coating can result in limited surface roughness and inadequate aluminum diffusion in the steel substrate. Conversely, big particles and/or thick coating can lead to uncontrolled roughness parameters and excessive diffusion depth of Al.

The alumina coating deposition based on the slurry of aluminum particles followed by consolidation treatment found commercial application, for example, in the *AlumiLok*^{TM} coating system offered by Nexceris, LLC as a 0.7 μm-thick Al_2O_3 coating (starting from around 44 μm Al particles) [13]. Ritucci et al. investigated the use of AlumiLokTM coating and its compatibility with glass–ceramic SOC sealants [14,15]. In the work of Frandsen et al. [16] an aluminization process using in-house prepared RAA slurry with alumina particles of 15 μm is reported and compared with the commercial *AlumiLok*^{TM} coating from Nexceris. The reduction of the Al particle size from 44 to 15 μm resulted in lower surface roughness (10–20 μm against 40–50 μm). However, it was found that the fracture energy calculated from the four-point bending test of the steel coated by the in-house Al slurry and joined with glass–ceramic sealant was 5 times higher compared to the commercial coating. The evidence suggested that the controlled surface roughness achieved by smaller Al powder positively influences the mechanical properties of the joined systems.

Si et al. [17] investigated the influence of the heat treatment process in the formation of the alumina coating, preparing a slurry for the RAA process with 44 μm-diameter Al particles, subsequently applied by brush painting on Crofer22H (4–5 mg/cm^2 of slurry). Performing heat treatments in air from 700 °C to 1000 °C allowed us to understand the mechanism of coating consolidation better, implementing the mechanism first proposed by Choi et al. [10]. At T <700 °C the liquid–solid interdiffusion between the liquid Al and the steel matrix is the main mechanism, at T = 700–900 °C the solid–solid interdiffusion between the Al-rich intermetallic compound and the steel matrix occurs, while at T >900 °C the growth of Al_2O_3 layer takes place. Therefore, increasing the temperature above 900 °C is recognized as the fundamental step to avoid excessive accumulation of aluminide compounds (with high CTE) and forming a continuous alumina layer, thanks to the reservoir effect offered by aluminum diffused into the steel at a lower temperature. The suitability of the same alumina-based coating on Crofer22H in joining with metallic Ag-based sealant was also evaluated [18,19].

Chou et al. [Y.-S. Chou, J.-P. Choi, J.W. Stevenson, Compliant alkali silicate sealing glass for solid oxide fuel cell applications: the effect of protective alumina coating on electrical stability in dual environment, Int. J. Hydrogen Energy (2012)] reported an alkali-containing compliant silicate sealing glass for SOFC applications, electrically evaluated in a dual environment with aluminized AISI441 substrates. Some interaction was observed at 800 °C, but no mechanical resistance of these interfaces was discussed. Mousa et al. [H. Mousa Mirabad, A. Nemati, M.A. Faghihi-Sani, M. Fakouri Hasanabadi, H. Abdoli, Effect of YSZ sol–gel coating on interaction of Crofer22 APU with sealing glass for solid oxide fuel/electrolysis cell, J. Alloys Compd (2020)] applied an 8YSZ coating on Crofer22 APU steel via sol–gel and dip-coating methods. The coating exhibited good thermal cycle stability and adhesion to the substrate, even after long-term heat treatment at 800 °C. While the coating showed excellent compatibility with the glass sealant, no mechanical assessment of the interfaces was presented. Sabato et al. [A.G. Sabato, A. Chrysanthou, M. Salvo, G. Cempura, F. Smeacetto, Interface stability between bare, MnCo spinel-coated AISI 441 stainless steel and a diopside-based glass–ceramic sealant, Int. J. Hydrogen Energy (2018)] examined the interaction of a diopside-based glass–ceramic with a MnCo spinel layer, using the EPD technique to deposit the MnCo layer. Good compatibility was achieved after 3500 h at 800 °C. The formation of (Mg,Cr,Mn)3O4 spinel at the sealant-oxide scale interface was observed, but it did not negatively affect the integrity between the sealant and the steel. In the present work, the EPD technique was used for the first time to form an alumina coating on Crofer22APU, simultaneously producing a corrugation on the Crofer surface. This increased surface roughness improved the overall interfacial resistance. The optimized suspension minimized material removal after sintering, resulting in low waste.

Electrophoretic deposition (EPD) is a fast, versatile, and adaptable coating technique. The low cost and low energy demand make EPD suitable for industrial applications. EPD has been used in various fields of traditional and advanced ceramics processing. However, only in the last few years has it emerged as a convenient coating method in processing corrosion-protective spinel coatings for energy conversion and storage applications [20–22]. However, the deposited layer's quality strongly depends on optimizing the various processing steps, starting from the suspension formulation, control of the deposition, and definition of possible post-deposition consolidation treatment. Electrophoretic deposition from suspensions of metallic powders is not widely reported in the literature: some of the main reasons can be found in the difficulty both in producing metallic particles in the colloidal range and in obtaining sufficient surface charge for non-oxide powders and avoiding agglomeration. However, the surface of metallic is normally passivated by forming an Al2O3 layer, presenting surface groups typical of oxides; moreover, metallic aluminum's density is lower than alumina's, making it possible to stabilize a suspension against sedimentation due to gravity.

The first elementary work on the EPD of Al particles was reported in 1963 by Pearlstein et al. [23], evaluating the amount of deposited powders in various organic medium mixtures. However, the topic has not found wide diffusion or practical application, and the limited number of published articles at the moment mostly concern the fabrication of thin films from nanopowders [24–28]. On the other hand, porous and thick (>200 μm) aluminum deposits were obtained by EPD on the metallic mesh using 5 μm-Al particles dispensed in ethanol and a considerable amount of polyacrylic acid and aluminum *iso*-propoxide as additives [29]. Few more available studies dealt with the identification of correlations between deposition parameters and deposited material amount; for example, Yang et al. [30] evaluated the influence of current density and deposition time on the deposition of aluminum particles in a solution of ethanol and aluminum chloride. Recently, Wagner et al. [31] reported a preliminary study of EPD of 2 μm-Al particles in the propan-2-ol medium, finding a correlation between the deposit thickness or porosity depending on deposition time and applied electric field. However, the mentioned works represent preliminary studies in the field and do not focus on the assessment of the deposition mechanisms nor on the possible post-deposition treatments to obtain alumina coatings for application in SOC technology.

Therefore, the present work aims to propose an innovative aluminization process achieved by EPD of metallic aluminum powder on Crofer22APU stainless steel. The study focuses on the optimization of the EPD deposition and the post deposition sintering treatments, finding correlations between the coating process and the morphological properties of the final alumina-based coating. The optimized coatings were used to produce joints with state-of-the-art glass-based sealants and 3YSZ electrolytes used in SOC technology devices. Joined samples were subjected to both static air ageing at 850 °C up to 1000 h to evaluate the interface evolution and the possible formation of corrosion products. Moreover, specific hourglass Crofer22APU joined samples were prepared to assess the mechanical resistance of the alumina-coated steel joints (both in an as-prepared state and after 1000-h aging) by torsion test.

With fast depositions and reusable aluminum suspensions, the EPD technique in the aluminization process would avoid the multistep process based on slurry preparation, without the need for an organic binder and allowing for controlled material usage. Apart from the application in SOC technology, the proposed aluminization process achieved by the EPD method represents a viable and convenient approach for any application where metallic substrates with complex features (tubes,

channels, fine patterns) need protection against oxidation.

No organic binders were used in the current aluminization process. As a result, there is no need to brush off residual shells, and the process is scalable to full-size applications. Calculations indicate that 22 ± 2 g/m^2 of aluminum powder is required to obtain the alumina coating. The material usage for the optimized suspension minimized material removal after sintering, resulting in a low amount of waste throughout the entire process. This optimization led to a cost reduction of approximately 20 % compared to the conventional process.

2. Experimental

2.1. Coatings preparation

The present study used unalloyed, atomised, spherical aluminum powder (supplied by Eckart Italia, purity ≥99.7 %, D50 1.1–1.5 μm) to prepare different EPD suspensions. Fig. 1a shows the XRD pattern collected on as-received powders with phase identification of a single-phase cubic aluminum (#01-089-2769 in PDF Database). SEM images reported in Fig. 1 b-c present the powder morphology. The mean particle diameter estimated by SEM image analysis using ImageJ software [32] among 300 particles corresponds to 0.96 μm.

Two EPD suspensions were optimised for the application of the steel aluminization process. The first suspension, in the following labelled as AlC3a, was obtained by dispersing 15 gL^{-1} of Al in 50 vol% acetone/50 vol% ethanol and 1 gL^{-1} I_2. The second suspension, labelled as AlC3b, was prepared in 100 vol% acetone, 1 gL^{-1} I_2 and 30 gL^{-1} of Al (i.e. double the solid load). Crofer22APU stainless steel [33] was used as the substrate for the depositions. For both suspensions, depositions were performed applying from 10 to 60 V, in a deposition time range from 10 to 60 s; moreover, in some cases, slight mechanical stirring was employed during deposition to avoid sedimentation. Sample-electrode distance was always maintained at 1.5 cm.

Eventually, EPD parameters were defined for both suspensions based on the homogeneity of the deposited green layer. Two optimal cases are presented in the present work: for the AlC3a suspension, 20 V for 30s was found; on the other hand, 55 V for 60s and slight mechanical stirring were used for the AlC3b. The suspensions and deposition parameters are summarized in Table 1. The two different suspensions determined the influence of the amount of deposited Al green layers on the final protective properties of the alumina coating after the thermal consolidation. To this purpose, the material usage was estimated by experimentally calculating the weight change by weighing before and after performing EPD for each suspension. At least ten steel coupons with an area of 1.5 × 1.5 cm^2 were considered for each set of samples. The materials deposited for AlC3b (62 ± 5 g/m^{-2}(−|-)) are remarkably higher than for AlC3a (22 ± 2 g/m^{-2}(−|-)), as expected from the higher solid content, higher deposition voltage, and longer time. The two proposed suspensions aimed to obtain coatings with different thicknesses and, therefore, to evaluate the influence on the final functional properties of the aluminization process.

After the deposition, the green samples were thermally treated to consolidate the coating. Both AlC3a and AlC3b samples were treated either at 1000 °C for 1 h in air (in the following labeled AlC3a@1000 and AlC3b@1000) or at 1100 for 30 min in air (in the following labeled AlC3a@1100 and AlC3b@1100) to evaluate the effect of temperature on coatings densification, aluminum diffusion, and Crofer22APU oxidation during treatment. In particular, the heat treatment time at 1100 °C was reduced to 30 min to preserve the steel substrate.

2.2. Samples characterization

The surface roughness of as-prepared coated samples was characterized with a stylus profilometer from Talysurf Intratouch, Taylor Hobson, USA). The different samples ' selected surface areas of 3 mm3 (2 mm x 1.5 mm) were scanned 205 times to obtain a 3D view of the surface. Data were analysed and refined using Gwyddion Software. The X-ray diffraction (XRD) patterns were obtained using a BrukerD8 diffractometer with Cu-Kα radiation; the patterns were recorded at room temperature in a 2Theta range of 10°−70°, with a step size of 0,013° and time per step of 100s; recorded patterns were analysed using HighScore Plus PANalytical software and JCPDS PDF-2 database. Hot Stage Microscope (HSM) analysis was performed to study the shrinkage of glass pellets on the modified steel surface during sintering (RT-1300 °C, 5 °C/min); glass pellets were cylindrically shaped compacted powder of the selected glass-based sealants. Data analysis was based on recording the projected images of the sample while heating. HSM analysis was in this case used to assess the wettability of the modified surfaces with the selected glass-based sealants to identify possible detrimental reactions during consolidation treatment.

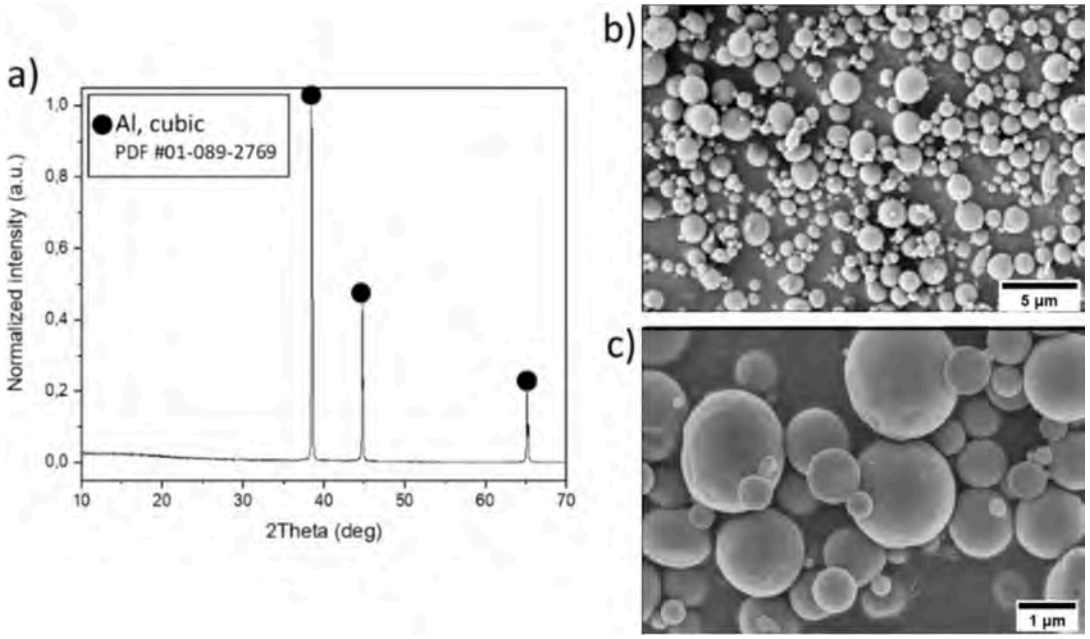

Fig. 1. Characterization of as-received al powder: xrd (a) and sem images at different magnifications (b and c).

Table 1
Summary of the two optimized coatings' EPD suspension and deposition parameters.

Label	Solvent [vol%]	I_2 [gL^{-1}]	Al [gL^{-1}]	Voltage [V]	Time [s]	Stirring	Material usage [$g/m^{-2}(-|-)$]
AlC3a	50 vol% EtOH 50 vol% Ace	1	15	20	30	No	22 ± 2
AlC3b	100 vol% Ace	1	30	55	60	Yes	62 ± 5

Surface modified steel samples were joined by using different glass–ceramic materials intended for SOC sealant applications: these materials were either strontium-containing silica-based glass-ceramics (with compositions and properties similar to those reported in [34], in the following text referred to as SiO_2-SrO-based glass sealant, for brevity) or barium-containing silica-based glass-ceramics (with composition and properties similar to those reported in [35] – in the following text referred as SiO_2-BaO-based glass sealant, for brevity).

The joined samples were obtained by sandwiching AlC3-coated Crofer22APU and 3YSZ sheets with the sealant material, followed by a thermal consolidation treatment in all the cases performed in air in the temperature range between 850 °C and 950 °C. For the samples used for aging in static air, pieces of 300 μm-thick 3YSZ spacers were placed between the steel and 3YSZ substrates to control the joint thickness better and to ensure the direct contact of studied materials with air during oxidation. Afterward, samples were aged in static air at 850 °C for 550 h.

The torsion test was conducted using hourglass-shaped Crofer22APU samples, identified as THG25. These samples have a circular joint area with a diameter of 25 mm and a square base of 30 mm, which facilitates easy torque loading. The sample design and test setup details can be found in references [36,37]. The test employed a custom-made torsion testing machine (Test Resources, Shakopee, MN, USA) available at J-tech@PoliTo laboratories. This machine is equipped with a 500 Nm torque cell, and the angular speed used during the tests was 2 degrees per minute.

For each sample, two AlC3a@1000-coated Crofer22APU hourglass samples were joined using a tape-casted foil of a silica-based barium-containing glass sealant. The glass is similar to HJ28 and has a silica content of 60 %, and the sum of glass modifiers (BaO + CaO + MgO) is approx. 30 %, where BaO is the primary modifier; more details can be found in ref [35]; According to SiO2-BaO binary phase diagram, the SiO2/(SiO2 + BaO) of 0.67 is required to obtain a BaSi2O5 phase. The BaSi2O5 phase has a CTE of 12–14.10^{-6} K^{-1}; therefore, obtaining a glass–ceramic sealant with a suitable CTE for SOEC applications is beneficial. Half of the obtained joined hourglass samples were exposed to oxidation in static air for 1000 h at 850 °C to compare the obtained shear stress values with those of the as-prepared samples. In total, 8 joined samples were tested.

After the torsion test, the shear strength of each sample has been calculated using the formula:

$$\tau_{max} = \frac{M_{max} * R}{J}$$

with,

$$J = \frac{\pi * R^4}{2}$$

Where τ_{max} represents the maximum shear strength the sample can withstand, M_{max} is the maximum torque, R is the radius of the circular joint area, and J is the polar moment of inertia.

Scanning electron microscopy (SEM) and Energy Dispersive X-ray spectroscopy (EDS) were employed to characterize the morphology and composition of samples in the top view and cross-section views of joined samples. For the cross-sections, samples were embedded in epoxy resin and polished up to 4000 SiC paper. Also, the optimised alumina coating was analysed by transmission electron microscopy (TEM). A FIB lamella for transmission electron microscopy analysis was prepared using NEON Cross- Beam 40EsB of ZEISS. TEM investigations were performed on high resolution, Titan Cubed G2 60–300 (FEI) – a probe Cs corrected (S) TEM, equipped with ChemiSTEM EDS system based on a four window-less Silicon Drift Detectors (Super X). STEM imaging was performed in high angle annular dark-field (HAADF) mode. Analysis of crystalline structure and phase composition was performed using the TEM-SAED method supported by JEMS software.

3. Results and discussion

3.1. Considerations on the electrophoretic deposition and the coating consolidation mechanisms

Electrophoretic deposition is mainly conducted using ceramic particles in the colloidal range, since they present hydroxyl groups on the surface that can easily react in acid/basic conditions or in the presence of a charger (e.g. iodine) to develop a surface charge. In the present study, metallic aluminum particles were used, and both the suspension stabilization and a deposition mechanism should be discussed. The EPD optimisation process allowed to identify of two suspensions as promising to obtain protective alumina coating on the stainless steel surface; in both cases, aluminum powders were dispersed in liquid media consisting of a solution of organic solvent (ethanol and/or acetone) and iodine, used as a surface charger. Acetone solutions using iodine as a surface charger are quite common in EPD processing [38]. When I_2 is dissolved in an acetone solution, four moles of free ions are generated from each mole of organic solvent, as described by the reaction in the following equation [39]:

$$CH_3 - CO - CH_3 + 2I_2 \leftrightarrow ICH_2 - CO - ICH_2 + 2H^+ + 2I^- \quad (1)$$

On the other hand, the use of ethanol with iodine is less reported in the literature; according to Zhu et al. [40] the possible reaction occurring is:

$$CH_3 - CH_2OH + I_2 \leftrightarrow ICH_2 - CH_2OH + H^+ + I^- \quad (2)$$

where 2 mol of free ions are produced from each mole of solvent (half moles compared to acetone).

The key aspect of the suspension stabilization was found in the fact that metallic aluminum always presents a partially oxidised external surface of alumina. Therefore, the protons generated by the reactions between the solvent and iodine, react with the hydroxyl groups on the oxidised shall of the particles, which overall develop a positive surface charge. Fig. 2 schematizes the possible mechanism of positive surface charge development for aluminum powders in the selected liquid media through the protonation of hydroxyl groups on the surface of the alumina shell of the particles.

After being stabilized in the suspension, Al particles need to be deposited by the effect of an applied electrical field through the suspension using two electrodes. For both AlC3a and AlC3b suspensions, the coatings deposited at the negatively polarised electrode, following a cathodic deposition mechanism. Besides the charged particles, free protons also move in the same direction, which is an inevitable side effect. According to a mechanism proposed by Hu et al. [41] for EPD of doped ceria, free protons are reduced at the cathode into H_2 and released as gas, while also reducing the pH of the suspension in proximity of the electrode. A similar process is likely to occur for reducing protonated Al

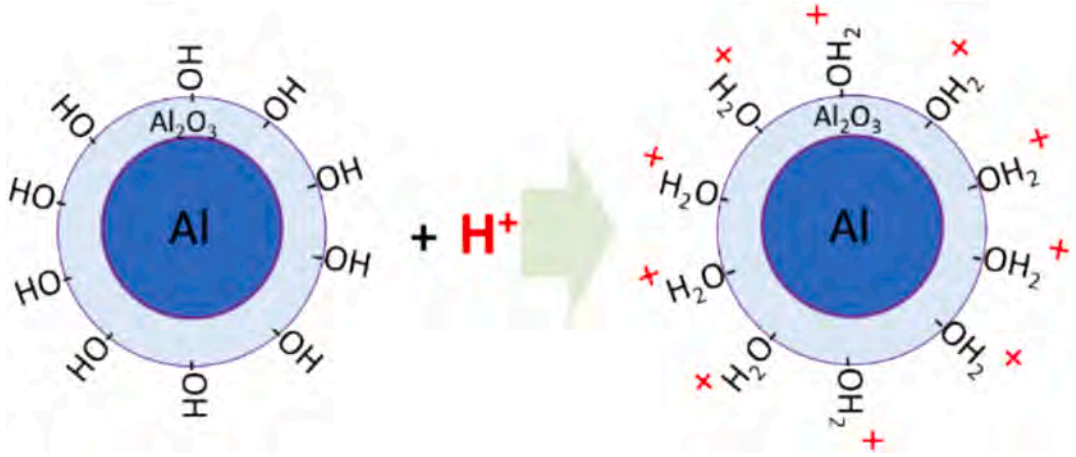

Fig. 2. Schematisation of aluminum particles' possible surface charge development mechanism.

particles once reach the electrode. Considering that the core of the particles in the suspension is metallic, it is possible to assume that electrons in the aluminum matrix interact according to the external electric field, modifying the charge distribution inside the particles. However, defining the potential implications of this effect would require further investigations. A schematic illustration of the proposed deposition mechanism is reported in Fig. 3.

Behind the deposition parameters, the post-deposition heat treatment plays a crucial role in achieving a protective and stable coating. During the heat treatment, the surface of all particles easily oxidizes, forming a thick alumina layer on the surface, but keeping the metallic form at the core. When exceeding the melting temperature of aluminum (i.e. 660.3 °C), the volumetric expansion of the liquid metal causes the external alumina shells to break. At the same time, the metallic Al partially diffuses in the steel substrate and continues with oxidation. At the end of the heating treatment, the surface of the steel substrate is coated with an alumina layer with increased surface roughness; debris of un-sintered coating can be found on the surface and removed by washing in ethanol in an ultrasonic bath and drying with compressed air. Fig. 4 schematizes the overall innovative aluminization process proposed.

The selected sintering parameters (1000 or 1100 °C) lead to the formation of α-Al_2O_3 layer on top of the Crofer22APU; typical XRD pattern collected on the obtained coatings is reported in Fig. 5 a with phase identification as included in the PDF Database: only peaks attributed to the steel substrate and Al_2O_3 layer are detected. The compatibility of the AlC3-coated steel with the glass–ceramic compositions employed was evaluated by Hot Stage Microscope (HSM), comparing glass shrinkage and sintering with the uncoated steel. Two typical HSM curves are displayed in Fig. 5 b: the curves of coated and uncoated Crofer22APU are similar, proving good compatibility of the sealant with the obtained alumina-based coating as well as the absence of major reactions (or crystallization phenomena which can hinder the viscous flow) between the alumina coated Crofer22APU and the glass.

3.2. *Surface characterization*

Fig. 6 a-d reports the SEM top view images, the 3D profilometer maps and surface roughness parameters of the four analysed cases for the proposed aluminization process. These comparisons for the different

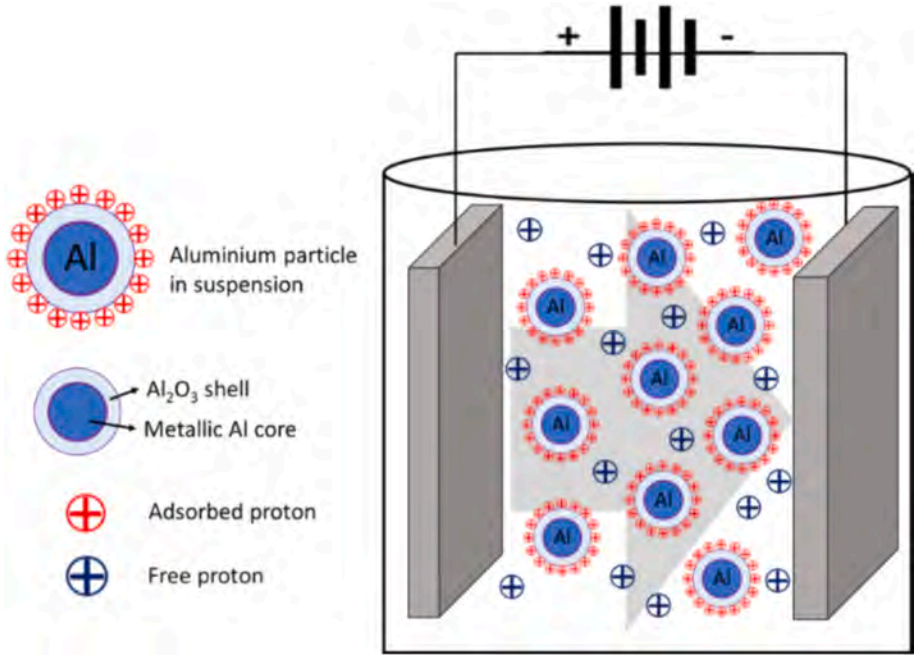

Fig. 3. Schematisation of the proposed deposition mechanism for aluminum particles.

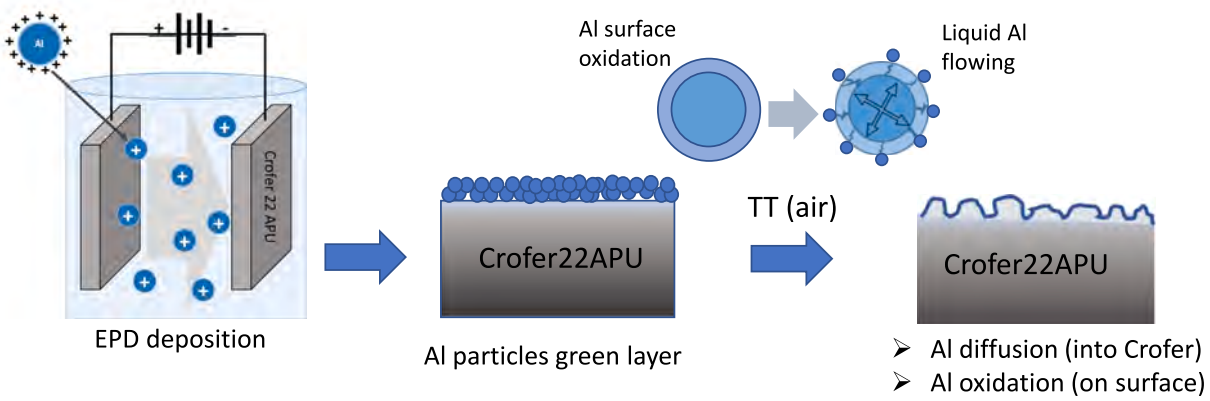

Fig. 4. Schematization of EPD process to obtain AlC3-coated Crofer22APU with enhanced roughness: electrophoretic deposition and thermal treatment.

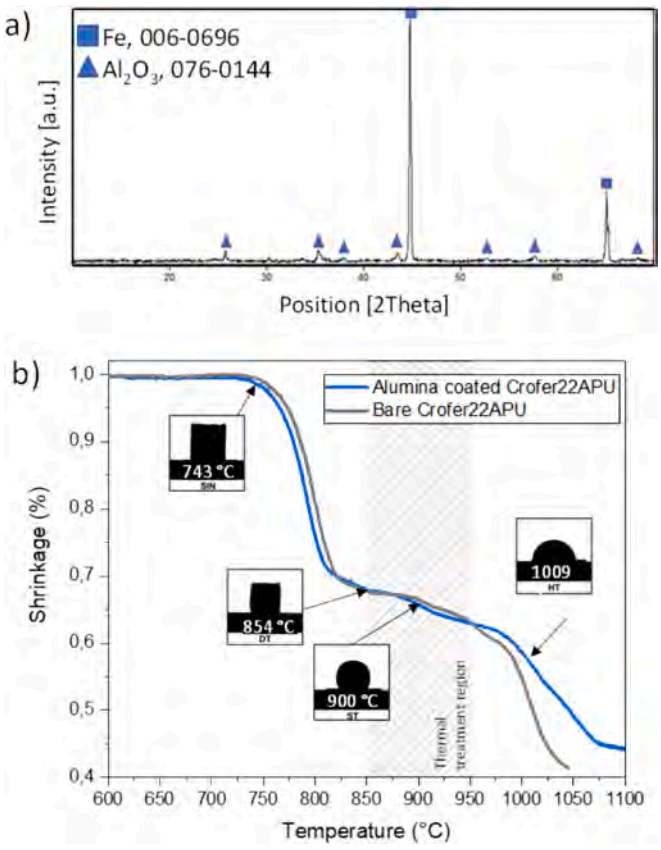

Fig. 5. Typical XRD pattern of AlC3 coated Crofer22APU (a) and comparison of shrinkage/temperature curve of a SiO_2-based glass sealant on AlC3 and bare Crofer22APU (b).

samples allowed us to understand the relationship between the surface properties and the parameters for the deposition and thermal consolidation of the coatings. Both AlC3a and AlC3b samples treated at 1000 °C present only a partially sintered external layer, where the shape of deposited particles is recognisable from the empty shells on the surface. On the other hand, the samples sintered at 1100 °C show a highly densified alumina layer on the top surface, as expected for the higher sintering temperature. The difference in surface densification is reflected in the roughness parameters: indeed, for both AlC3a and AlC3b coatings, higher roughness was obtained at lower sintering temperatures (i.e., 1000 °C). Independently from the sintering temperature, AlC3b samples present higher average surface roughness (Sa) and peak height (Sp) compared to AlC3a samples. This is likely due to the higher quantity of deposited layer and thicker coating for AlC3b suspension.

Fig. 7 reports SEM cross-section images of the four investigated aluminization coatings variants; in these cases, the coated Crofer22APU samples after thermal consolidation were joined with a silica-based sealant to investigate possible reactions with the joining materials. In none of the analysed samples, any unwanted phase formation (e.g. barium or strontium chromates) was found after the joining treatment, as visible in Fig. 7. AlC3a samples present around 1 μm-thick alumina layer with a corrugated appearance. However, the AlC3a@1100 exhibits an around 5 μm-thick layer of densified alumina debris between the alumina coating and the sealant (Fig. 7 b): this feature explains the lower average surface roughness measured for this samples (Fig. 6 b) compared to the same coating sintered at 1000 °C. The AlC3b coating results in thicker (i.e. around 2 μm), as expected from the higher amount of material deposited during EPD (see Table 1). The coating results well continuous for the AlC3b@1000 (Fig. 7 c), but discontinuous and covered with densified alumina debris for AlC3b@1100 (Fig. 7 d), which also expresses the higher degree of internal steel oxidation due to the treatment temperature. A treatment at a higher temperature (i.e. 1100 °C) caused partial internal oxidation of the steel: the distribution of the internal oxide is visible throughout the substrate, between 3 to 5 μm deep. Then, the steel is generally homogeneously covered by a well-defined alumina layer (EDS not reported here), which also follows the rough profile of the substrate. However, two more areas are visible at the interface with the glass–ceramic sealant. First, Cr, Mn and Fe could have likely diffused during the treatment, forming a mixed oxide with Al. Moreover, the whole surface is covered by a thick alumina layer. Therefore, consolidating the alumina coating at 1100 °C appears detrimental from multiple points of view.

During the thermal consolidation treatment, part of the molten aluminum diffuses inside the steel surface. First, SEM EDS analysis was performed to evaluate the Al diffusion depth, which reached 5 to 10 μm inside the Crofer22APU substrate. A more accurate assessment was conducted by TEM investigation from lamella of the AlC3a-coated Crofer22APU. Fig. 8 reports the EDS elemental maps of the AlC3a@1000 lamella, showing the first 5 μm from the steel external surface. The coating-steel surface appears extremely complex due to the development of multiple oxide phases with different compositions. Together with the external alumina shell (around 2 μm from the external surface), grains of mixed iron-chromium, iron-manganese-chromium, iron-manganese-chromium-alumina oxides and chromia were detected by TEM-EDS analyses till around 5 μm from the external surface.

3.3. Static air aging at 850 °C

Fig. 9 shows cross-section SEM images of bare (a-b), AlC3a@1000-coated (c-d), and AlC3b@1000-coated (e-f) Crofer22APU joined with a silica-based glass–ceramic sealant after aging at 850 °C for 550 h.

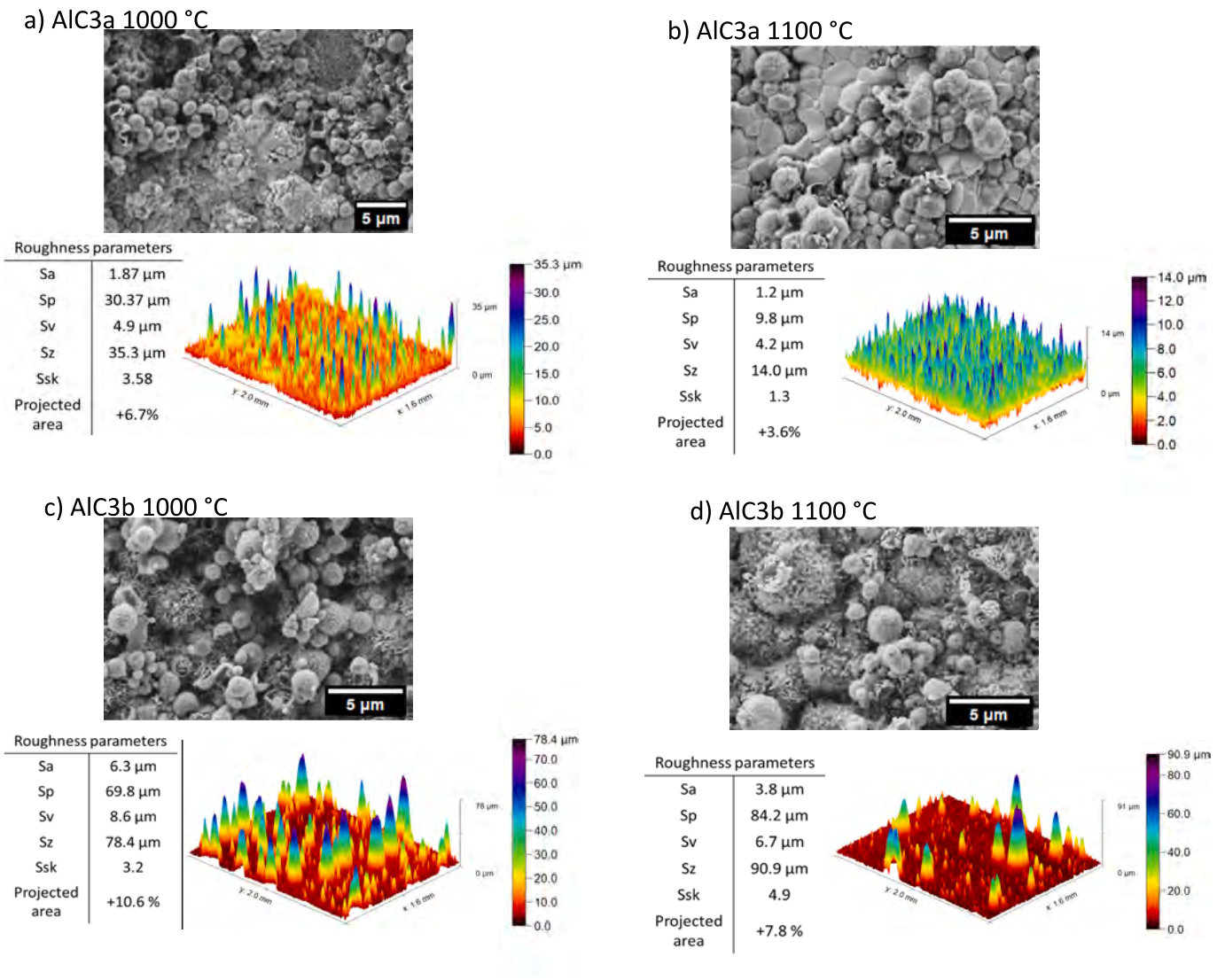

Fig. 6. SEM top view images, roughness parameters and 3D profilometer maps of Alc3a@1000 (a), AlC3a @1100 (b), AlC3b@1000 (c) and AlC3b@1100 (d).

As visible in SEM images in Fig. 9 a-b for the joint with bare Crofer22APU, the external surface of the sealant exposed to air during aging developed a continuous layer of chromates, on average 15 µm-thick. The evidence proves that Cr continuously evaporated from the bare steel at the side during aging, redepositing and reacting with the glass–ceramic sealant. The formation of chromates is particularly evident at the steel/sealant/air boundary, together with apparent steel oxidation both at the external part of the joint and at the interface with the steel. Degradation phenomena starting at the steel/sealant/air boundary can propagate at the steel/sealant interface, influencing the soundness of the joined system. Indeed, the significant formation of Ba-chromates is also evident at the steel/sealant interface inside the joint till around 300 µm from the air side. This feature is better visible in Fig. 9 b, where an oxide scale composed of Ba-chromates, Mn-Cr spinel and chromia on the top of the Crofer22APU surface is identified.

On the other hand, the joint with AlC3a@1000-Crofer22APU (Fig. 9 c-d) developed minimal formation of chromates on the sealant at the interface with air and only in a few zones with around 2- to 5 µm thickness. Unlike bare Crofer22APU joined samples, only slight chromate formations are visible closer to the steel substrate at the sealant/air interface. The evidence proves the effectiveness of the proposed AlC3a coating in reducing the Cr evaporation rate from the steel substrate and its re-condensation on the sealant surface. Fig. 9 d shows no chromates developed at all at the metal/sealant interface for the AlC3a-coated Crofer22APU joint after aging. Moreover, AlC3a coating maintained a similar morphology to the as-prepared sample: the coating is continuous, and the steel surface roughness is preserved. Despite the aging time, no evident signs of reactions occurring between the coating and the sealant are appreciable after aging, as the interface is sound, without the formation of secondary phases or porosity.

SEM cross-section images of aged joint obtained with AlC3b@1000-Crofer22APU are reported in Fig. 9 e-f. From the image at lower magnification, a small degree of chromate formation at the sealant/air interface is appreciable, and most chromates accumulated in the sealant area closer to the steel substrate. The internal interface between the coated Crofer22APU and the sealant does not show the formation of secondary phases. Still, the AlC3b coating is continuous and maintains the highly corrugated morphology typical of the as-prepared samples. The minimal internal oxidation of the steel proves the good protection capability of the AlC3b coating and the similar capability in reducing Cr evaporation to the AlC3a coating. However, a notable development of pores at the metal/sealant interface occurred. The reason for this would require additional investigation, for example, to define a potential correlation between the EPD process, sintering, and morphology evolution during aging. Therefore, AlC3b coating does not present good reliability as a protective coating, unless further optimization steps were carried

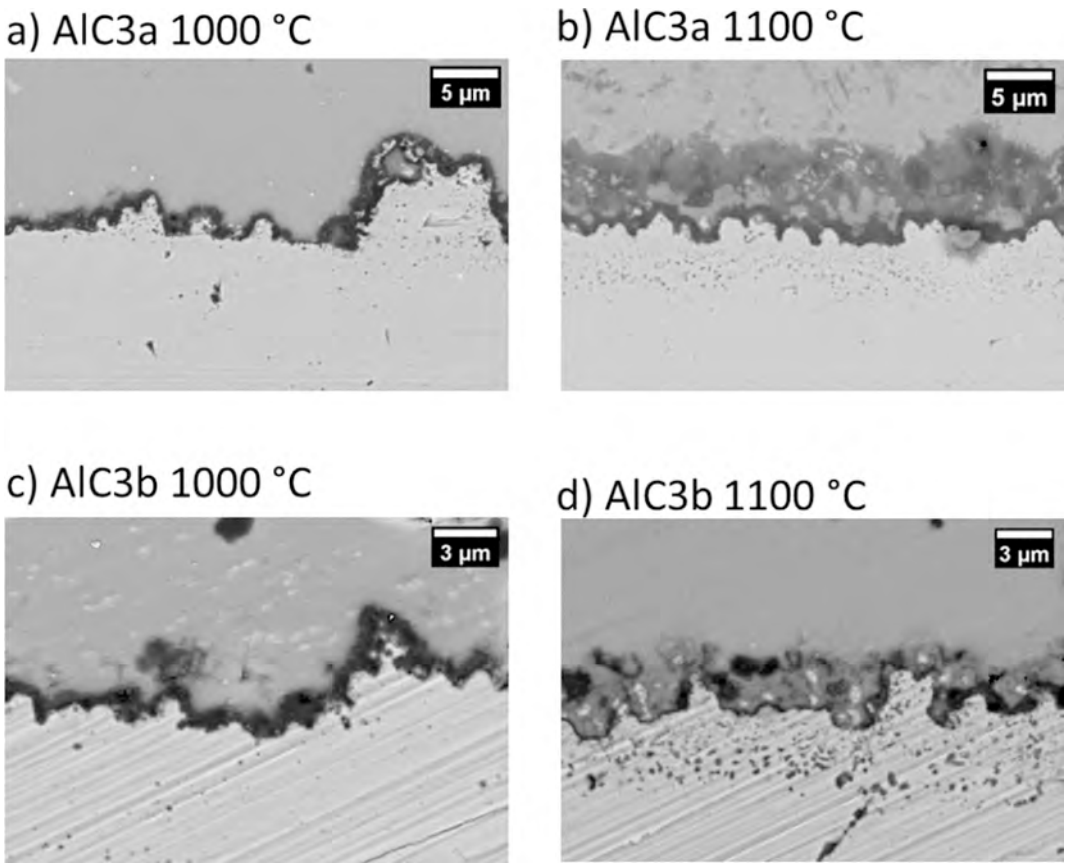

Fig. 7. SEM cross section images of AlC3-coated Crofer22APU and joined with a silica glass-based sealants for SOC applications: AlC3a@1000 (a), AlC3a@1100 (b), AlC3b@1000 (c) and AlC3b@1100.

out.

3.4. Mechanical properties of joined samples: Torsion test

The visual inspection of AlC3a@1000-Crofer22APU hourglass for as-prepared and aged samples inside the torsion machine immediately after testing is shown in Fig. 10 a and b respectively. As visible in the reported pictures, a cohesive fracture mode was observed in both cases: indeed, part of the glass–ceramic sealant was attached on both sides of the fractured samples in all tested samples. On the other hand, a recent study demonstrated that bare Crofer22APU hourglass samples joined with a similar silica-based glass–ceramic sealant expresses an adhesive fracture mode, which indicates a weak sealant/interconnect interface, and with an average shear strength of 24.0 ± 6 MPa (as-prepared samples) [36]. Regarding the calculated shear strength, both sets of samples in the present study expressed very similar values: on average 31.2 ± 2.0 MPa and 33.0 ± 1.0 MPa for as-prepared and aged samples, respectively. The evidence indicates that during the 1000 h-aging no detrimental reactions occurred at the AlC3a-coated Crofer22APU/sealant interface that could negatively affect the mechanical resistance of the joint. The calculated standard deviations are low compared to results reported in the literature on the same field, even if very few studies are available for comparison.

Regarding the calculated shear strength, both sets of samples in the present study expressed very similar values: on average, 31.2 ± 2.0 MPa and 33.0 ± 1.0 MPa for as-prepared and aged samples, respectively. The evidence indicates that during the 1000 h-aging, no detrimental reactions occurred at the AlC3a-coated Crofer22APU/sealant interface that could negatively affect the mechanical resistance of the joint. The calculated standard deviations are low, but as reported in [M. Fakouri Hasanabadi, J. Malzbender, S.M. Groß-Barsnick, H. Abdoli, A.H. Kokabi, M.A. Faghihi-Sani, Finite element optimization of sample geometry for measuring the torsional shear strength of glass/metal joints, Volume 46, Issue 4, March 2020, 4857–4863] the values are reasonable since a symmetric configuration of specimen has been adopted which can promote a uniform stress distribution across the joint, reducing a lot the standard deviations of the results.

For example, torsional test results on alumina-coated Crofer22APU were already reported by De La Pierre et al. [37], where the steel substrate was first modified by deposition of aluminum powder by hand-coating and afterwards joined with a diopside-based glass–ceramic sealant. In that case, 40 ± 6 MPa and 34 ± 6 MPa shear strength values were obtained for as-prepared and aged (700 h at 750 °C) samples, respectively: the values reside in the same range of the present study, despite the different glass-system employed.

Fig. 10 c and d show SEM cross-section images with EDS elemental analysis of marked areas of aged AlC3a-coated half-hourglass after the torsion test. A highly dense glass–ceramic layer 140 to 90 µm-thick is well visible throughout the samples, confirming the occurrence of a cohesive fracture mode propagation. At the metal-sealant interface, the AlC3a coating is well visible as a continuous layer on the Crofer22APU substrate and maintains the rough surface typical of as-prepared samples. The EDS analysis demonstrated that Al remains in a diffused layer of around 5-µm beneath the steel surface. Although internal oxidation in the steel substrate is not visible at this magnification, EDS analysis in areas 1 and 2 revealed the presence of aluminum and oxygen, suggesting possible small alumina formation from the metallic aluminum first diffused inside the steel. Comparing these findings with other studies in the literature confirms that the EPD technique is a viable, low-cost method for achieving proper surface modification of metallic interconnects. Additionally, the torsion test on hourglass-shaped specimens proves to be a convenient and promising method for assessing

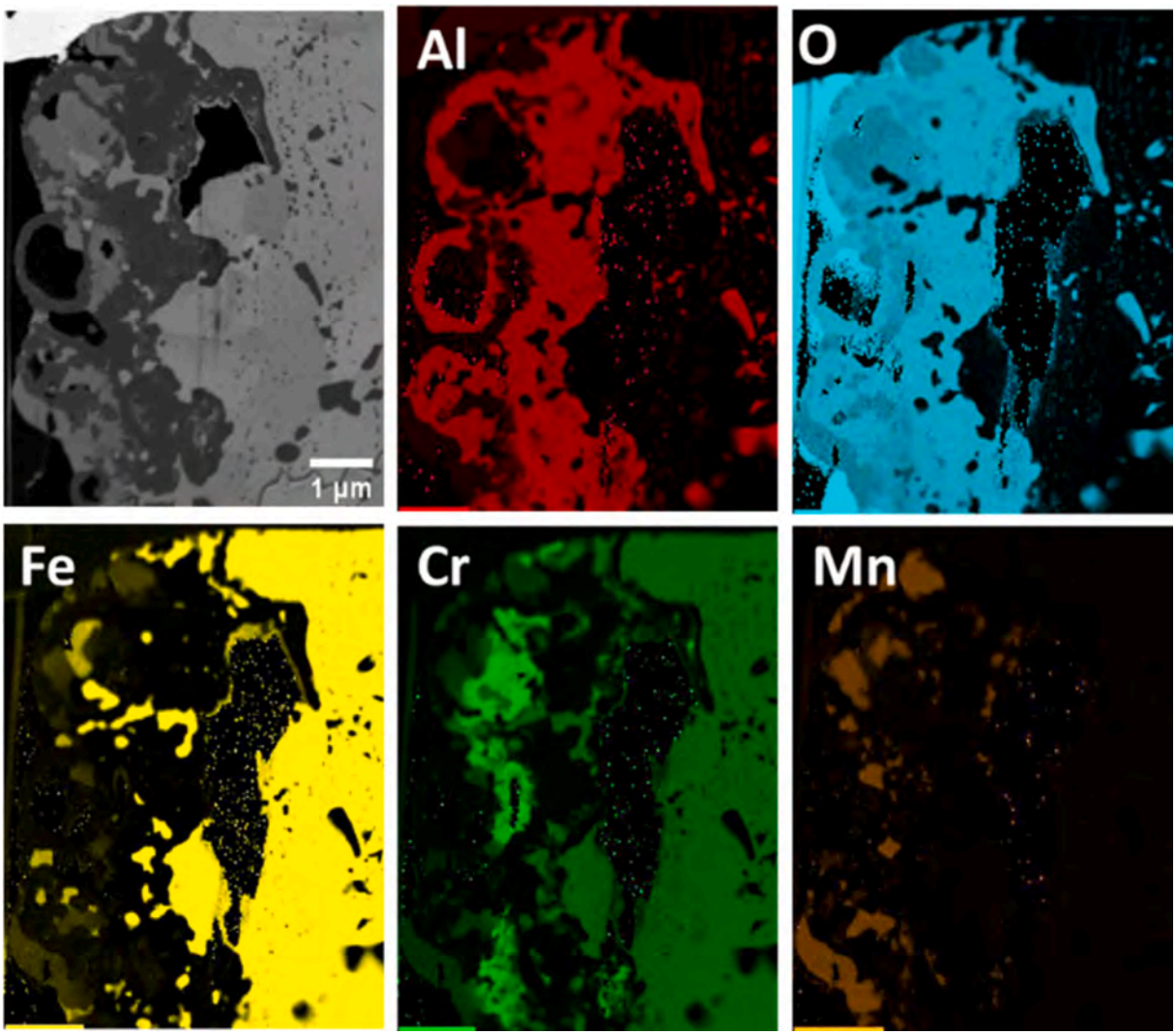

Fig. 8. TEM EDS elemental map of AlC3a@1000 lamella.

shear strength with minimal influence from additional stress components, thereby providing valuable data for designing novel interfaces.

4. Conclusions

The present study aimed to propose an innovative steel aluminization process through EPD and to highlight the influence of processing parameters in defining the coating properties – here, AlC3. Two EPD suspensions containing metallic aluminum particles were optimised regarding composition and deposition parameters. The deposited samples were subjected to different thermal consolidation treatments (at 1000 and 1100 °C) to assess the densification of the coating. The morphological characterization allowed us to find specific correlations between the EPD processing (i.e. suspension preparation, deposition voltage, and time), the post deposition thermal consolidation, and the features (i.e. average roughness, peaks distribution, and coating densification) of the obtained alumina coating.

Sintering the coating at 1100 °C could induce excessive coating densification, resulting in low average surface roughness and internal oxidation of the steel subscale. The AlC3b coating is thick, resulting in increased average surface roughness and higher material consumption; studies conducted so far have not clarified the possible detrimental phenomenon due to a corrugated surface and uncontrolled Al diffusion inside the steel substrate. Therefore, a thinner AlC3a coating consolidated at 1000 °C for 1 h was selected as the best candidate for the steel aluminization process.

The static-air aging at 850 °C demonstrated that the alumina coating offers a barrier against ions diffusion between the steel and the sealant, limiting undesired reactions at high temperatures. Moreover, the corrugated morphology of the alumina coating offers a better mechanical interlocking with the sealing material. Indeed, the torsion tests performed on AlC3a@1000-coated Crofer22APU proved that the AlC3 coating strengthens the metal-ceramic interface, leading to cohesive fracture of the hourglass-shaped joined samples. The obtained shear strength values were 31.2 ± 2.0 MPa and 33.0 ± 1.0 MPa for as-prepared and aged samples, respectively, indicating no interface degradation after 1000-h aging and high reproducibility.

Overall, the use of the EPD technique in the aluminization process would avoid the multistep process based on slurry preparation, without the need for an organic binder and allowing for controlled material usage. Also, the EPD method presents the advantage of fast depositions and reusable aluminum suspensions.

Apart from application in SOC technology, the proposed EPD-aluminization process represents an innovative and convenient approach for any application where metallic substrates with complex features (tubes, channels, fine patterns) need protection against oxidation.

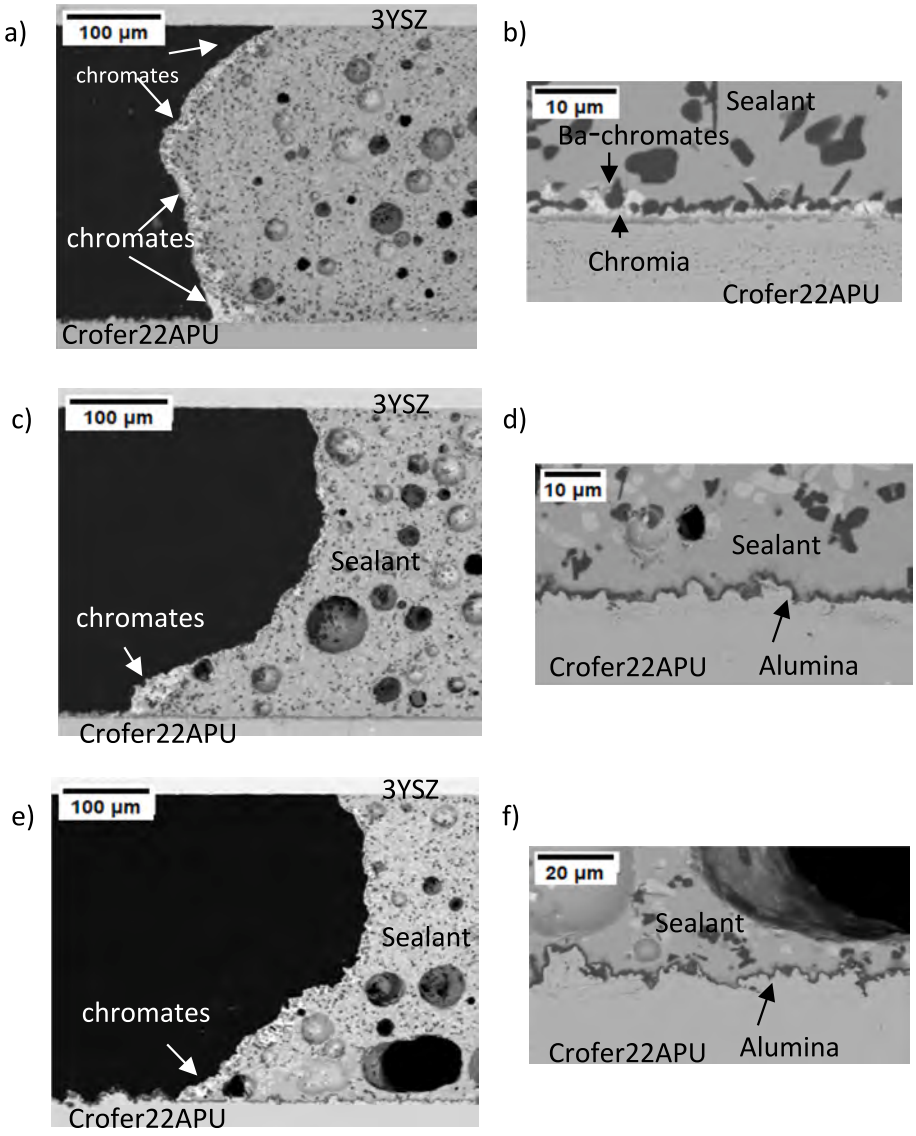

Fig. 9. SEM cross section images of bare (a-b), AlC3a@1000-coated (c-d), and AlC3b@1000-coated (e-f) Crofer22APU joined with a silica-based glass ceramic sealant after thermal oxidation at 850 °C for 550 h.

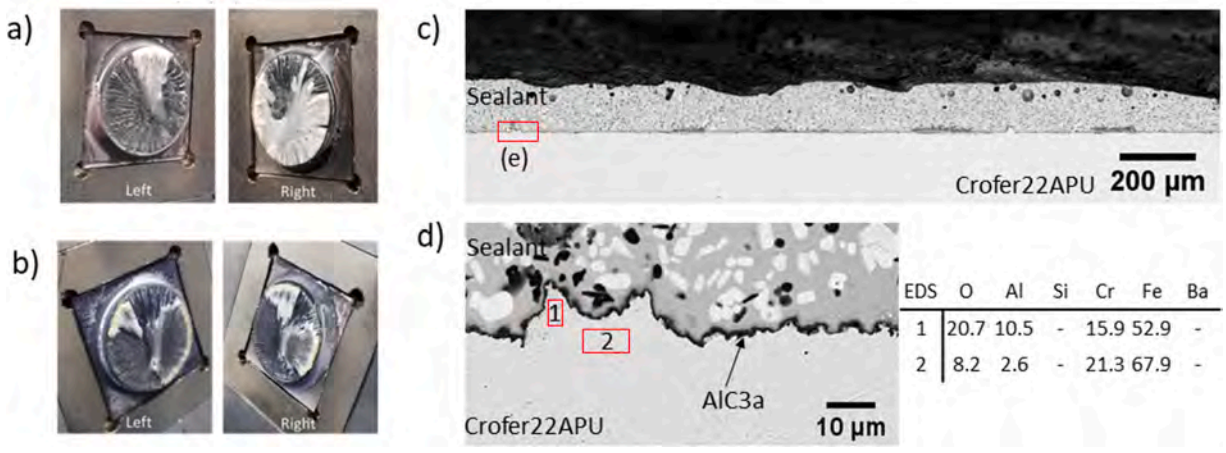

Fig. 10. Visual inspection of as-prepared (a) and aged (b) AlC3a@1000-Crofer22APU joined samples inside the torsion machine immediately after testing. Sem cross-section images of AlC3a@1000-Crofer22APU sample aged at 850 °C for 1000 h after torsion test (d-e).

CRediT authorship contribution statement

E. Zanchi: Writing – original draft, Methodology, Investigation, Data curation, Conceptualization. **H. Javed:** Validation. **S.De La Pierre:** Investigation, Data curation. **M. Ferraris:** Resources. **G. Cempura:** Investigation, Data curation. **A. Benelli:** Data curation. **A.R. Boccaccini:** Conceptualization. **F. Smeacetto:** Writing – review & editing, Validation, Supervision, Conceptualization.

Declaration of competing interest

The authors declare that they have no known competing financial interests or personal relationships that could have appeared to influence the work reported in this paper.

Acknowledgments

The research leading to this work partially received funding from:

-the European Commission's Fuel Cells Hydrogen Joint Undertaking (FCH 2 JU), grant agreement No 874577 – NewSOC.

- The EU HORIZON-JU-CLEANH2-2022, grant agreement 101101274-HyP3D.

The funding from the European Union's Horizon 2020 research and innovation program, Grant Agreement No. 823717 ESTEEM3 – Ceram-ECS and Glamater, is acknowledged.

KMM-VIN European Virtual Institute on Knowledge-based Multi-functional Materials AISBL is acknowledged for providing fellowships and infrastructure.

J-Tech at Politecnico di Torino and Eckart Italia are acknowledged for the torsion tests and for providing the aluminum powder used in the study.

Data availability

The authors are unable or have chosen not to specify which data has been used.

References

[1] V.A.C. Haanappel, V. Shemet, S.M. Gross, T. Koppitz, N.H. Menzler, M. Zahid, W. J. Quadakkers, Behaviour of various glass-ceramic sealants with ferritic steels under simulated SOFC stack conditions, J. Power Sources 150 (2005) 86–100, https://doi.org/10.1016/j.jpowsour.2005.02.015.

[2] N. Lahl, D. Bahadur, K. Singh, L. Singheiser, K. Hilpert, Chemical interactions between aluminosilicate base sealants and the components on the anode side of solid oxide fuel cells, J. Electrochem. Soc. 149 (2002) A607, https://doi.org/10.1149/1.1467945.

[3] Y.-S. Chou, J.W. Stevenson, J.-P. Choi, Alkali effect on the electrical stability of a solid oxide fuel cell sealing glass, J. Electrochem. Soc. 157 (2010) B348, https://doi.org/10.1149/1.3275744.

[4] Y.-S. Chou, J.W. Stevenson, P. Singh, Novel refractory alkaline earth silicate sealing glasses for planar solid oxide fuel cells, J. Electrochem. Soc. 154 (2007) B644, https://doi.org/10.1149/1.2733868.

[5] A. Rost, J. Schilm, M. Kusnezoff, A. Michaelis, Degradation of sealing glasses for SOFC under electrical load and dual atmosphere, J. Ceram. Sci. Technol. 3 (2012) 69–80, https://doi.org/10.4416/JCST2012-00002.

[6] C. Thieme, C. Rüssel, Interfacial reactions between a crystallizing sealing glass from the system BaO–ZnO–NiO–SiO2 and Crofer 22 APU, J. Mater. Sci. 51 (2016) 756–765, https://doi.org/10.1007/s10853-015-9398-x.

[7] Z. Yang, G. Xia, K.D. Meinhardt, S.K. Weil, J.W. Stevenson, Chemical stability of glass seal interfaces in intermediate temperature solid oxide fuel cells, J. Mater. Eng. Perform. 13 (2004) 327–334, https://doi.org/10.1361/10599490419298.

[8] Y.S. Chou, J.W. Stevenson, P. Singh, Effect of pre-oxidation and environmental aging on the seal strength of a novel high-temperature solid oxide fuel cell (SOFC) sealing glass with metallic interconnect, J. Power Sources 184 (2008) 238–244, https://doi.org/10.1016/j.jpowsour.2008.06.020.

[9] Y.-S. Chou, J.W. Stevenson, P. Singh, Effect of aluminizing of Cr-containing ferritic alloys on the seal strength of a novel high-temperature solid oxide fuel cell sealing glass, J. Power Sources 185 (2008) 1001–1008, https://doi.org/10.1016/j.jpowsour.2008.09.004.

[10] J.P.J. Choi, Y.S. Chou, J.W. Stevenson, Reactive Air Aluminization PNNL-20859 (2011).

[11] J.-P. Choi, J.W. Stevenson, K.S. Weil, Y.-S.-M. Chou, J.T. Darsell, V.V. Joshi, Reactive coating processes, US 10378094 (2019) B2.

[12] J.P. Choi, K.S. Weil, Y.M. Chou, J.W. Stevenson, Z.G. Yang, Development of MnCoO coating with the new aluminizing process for planar SOFC stacks, Int. J. Hydrog. Energy 36 (2010) 4549–4556, https://doi.org/10.1016/j.ijhydene.2010.04.110.

[13] N.J. Kidner, ALUMILOKTM COATINGS: ENHANCED HIGH TEMPERATURE PERFORMANCE FOR COMMERCIAL STEELS, Nexceris LLC (n.d.) 1–5. https://nexceris.com/wp-content/uploads/2019/08/AlumiLok-Coatings-Enhanced-High-Temperature-Performance-for-Commercial-Steels.pdf (accessed December 8, 2023).

[14] I. Ritucci, R. Kiebach, B. Talic, L. Han, P. Zielke, P.V. Hendriksen, H.L. Frandsen, Improving the interface adherence at sealings in solid oxide cell stacks, J. Mater. Res. 34 (2019) 1167–1178, https://doi.org/10.1557/jmr.2018.459.

[15] I. Ritucci, K. Agersted, P. Zielke, A.C. Wulff, P. Khajavi, F. Smeacetto, A.G. Sabato, R. Kiebach, A Ba-free sealing glass with a high coefficient of thermal expansion and excellent interface stability optimized for SOFC/SOEC stack applications, Int. J. Appl. Ceram. Technol. 15 (2018) 1011–1022, https://doi.org/10.1111/ijac.12853.

[16] H.L. Frandsen, I. Ritucci, P. Khajavi, B. Talic, R. Kiebach, P.V. Hendriksen, Enhancing the robustness of brittle solid oxide cell stack components, ECS Trans. 91 (2019) 2201–2211, https://doi.org/10.1149/09101.2201ecst.

[17] X. Si, C. Li, Y. Bo, J. Qi, J. Feng, J. Cao, The role of Al diffusion behavior in the process of forming a super-reliable Al2O3 protective layer during reactive air aluminization, Appl. Surf. Sci. 518 (2020) 146242, https://doi.org/10.1016/j.apsusc.2020.146242.

[18] X. Si, J. Cao, I. Ritucci, B. Talic, J. Feng, R. Kiebach, Enhancing the long-term stability of Ag based seals for solid oxide fuel/electrolysis applications by simple interconnect aluminization, Int. J. Hydrog. Energy 44 (2019) 3063–3074, https://doi.org/10.1016/j.ijhydene.2018.11.071.

[19] W.L. Zhou, S.P. Hu, M.J. Yang, Y. Luo, W. Fu, X.G. Song, Reactive air brazing of 3YSZ ceramic to aluminized Crofer22H stainless steel using Ag–CuO fillers, Int. J. Appl. Ceram. Technol. 19 (2022) 2367–2378, https://doi.org/10.1111/ijac.14035.

[20] E. Zanchi, A.G. Sabato, M.C. Monterde, L. Bernadet, M. Torrell, J.A. Calero, A. Tarancón, F. Smeacetto, Electrophoretic deposition of MnCo2O4 coating on solid oxide cell interconnects manufactured through powder metallurgy, Mater. Des. 227 (2023) 111768, https://doi.org/10.1016/j.matdes.2023.111768.

[21] E. Zanchi, J. Ignaczak, S. Molin, G. Cempura, A.R. Boccaccini, F. Smeacetto, Electrophoretic co-deposition of Mn1.5Co1.5O4, Fe2O3 and CuO: Unravelling the effect of simultaneous addition of Cu and Fe on the microstructural, thermo-mechanical and corrosion properties of in-situ modified spinel coatings for solid oxide cell interconnects, J. Eur. Ceram. Soc. 42 (2022) 3271–3281, https://doi.org/10.1016/j.jeurceramsoc.2022.02.008.

[22] E. Zanchi, A.G. Sabato, H. Javed, A. Drewniak, D. Koszelow, S. Molin, F. Smeacetto, Ceramic Coatings for Metallic Interconnects and Metal Alloys Support for Solid Oxide Electrolysis Applications, in: M.A. Laguna-Bercero (Ed.), High Temp. Electrolysis, Springer International Publishing, Cham, 2023: pp. 117–151. https://doi.org/10.1007/978-3-031-22508-6_6.

[23] F. Pearlstein, R. Wick, A. Gallaccio, Electrophoretic deposition of metals, J. Electrochem. Soc. 110 (1963) 843, https://doi.org/10.1149/1.2425882.

[24] Z. Xu, D. Jiang, Z. Wei, J. Chen, J. Jing, Fabrication of superhydrophobic nano-aluminum films on stainless steel meshes by electrophoretic deposition for oil-water separation, Appl. Surf. Sci. 427 (2018) 253–261, https://doi.org/10.1016/j.apsusc.2017.08.189.

[25] X. Guo, T. Liang, J. Wang, X. Li, Facilely electrophoretic derived aluminum/zinc (II) oxide nanocomposite with superhydrophobicity and thermostability, Ceram. Int. 46 (2020) 1052–1058, https://doi.org/10.1016/j.ceramint.2019.09.071.

[26] D. Zhang, X. Li, B. Qin, C. Lai, X. Guo, Electrophoretic deposition and characterization of nano-Al/Fe 2O3 thermites, Mater. Lett. 120 (2014) 224–227, https://doi.org/10.1016/j.matlet.2014.01.113.

[27] K. Luo, N. Shi, H. Cong, C. Sun, Electrophoretic deposition of nickel, iron and aluminum nanoparticles on carbon fibers, J. Solid State Electrochem. 10 (2006) 1003–1007, https://doi.org/10.1007/s10008-005-0044-4.

[28] E.S. Leonenko, L.I. Sorokina, R.M. Ryazanov, E.A. Lebedev, Features of electrophoretic formation of local heat sources based on nanosized powder Al, J. Phys. Conf. Ser. 2086 (2021), https://doi.org/10.1088/1742-6596/2086/1/012192.

[29] K.S. Yang, Z. Jiang, J.S. Chung, Electrophoretically Al-coated wire mesh and its application for catalytic oxidation of 1,2-dichlorobenzene, Surf. Coat. Technol. 168 (2003) 103–110, https://doi.org/10.1016/S0257-8972(02)00569-8.

[30] L. Yang, X. Wu, D. Weng, Development of uniform and porous Al coatings on FeCrAl substrate by electrophoretic deposition, Colloids Surf. Physicochem. Eng. Asp. 287 (2006) 16–23, https://doi.org/10.1016/j.colsurfa.2006.03.016.

[31] J. Wagner, C. Josse, L. Gani, S. Knittel, P.-L. Taberna, F. Ansart, Electrophoretic deposition of aluminum particles from pure propan-2-ol suspensions, Results Mater. 13 (2022) 100259, https://doi.org/10.1016/j.rinma.2022.100259.

[32] C.A. Schneider, W.S. Rasband, K.W. Eliceiri, NIH Image to ImageJ: 25 years of image analysis, Nat. Methods 9 (2012) 671–675.

[33] VDM-Metals, Crofer 22 APU Material Data Sheet, (2010).

[34] H. Javed, E. Zanchi, F. D'Isanto, C. Bert, D. Ferrero, M. Santarelli, F. Smeacetto, Novel SrO-containing glass-ceramic sealants for solid oxide electrolysis cells (SOEC): Their design and characterization under relevant conditions, Materials 15 (2022) 5805, https://doi.org/10.3390/ma15175805.

[35] H. Javed, A.G. Sabato, M. Mansourkiaei, D. Ferrero, M. Santarelli, K. Herbrig, C. Walter, F. Smeacetto, Glass-ceramic sealants for SOEC: Thermal characterization and electrical resistivity in dual atmosphere, Energies 13 (2020) 3682, https://doi.org/10.3390/en13143682.

[36] F. Smeacetto, E. Zanchi, D. Meena Narayana Menon, D. Janner, S. Lamnini, M. Salvo, S. De La Pierre, H. Javed, M. Ferraris, Torsional behaviour of glass-

joined, laser-processed Crofer 22 APU interconnect: Unravelling the effect of surface roughness on the shear strength, Ceram. Int. 48 (2022) 32837–32843, https://doi.org/10.1016/j.ceramint.2022.07.210.
[37] S. De La Pierre, M. Ferraris, I. Ritucci, R. Kiebach, H. Lund Frandsen, D. Ferrero, F. Smeacetto, Torsional behaviour of a glass-ceramic joined alumina coated Crofer 22 APU steel, Ceram. Int. 48 (2022) 25368–25373, https://doi.org/10.1016/j.ceramint.2022.05.210.
[38] L. Besra, M. Liu, A review on fundamentals and applications of electrophoretic deposition (EPD), Prog. Mater. Sci. 52 (2007) 1–61.
[39] T. Mathews, Fabrication of La1−xSrxGa1−yMgyO3−(x+y)/2 thin films by electrophoretic deposition and its conductivity measurement, Solid State Ion. 128 (2000) 111–115, https://doi.org/10.1016/S0167-2738(99)00308-2.
[40] H. Zhu, S. Geng, G. Chen, F. Wang, Electrophoretic deposition of trimanganese tetraoxide coatings on Ni-coated SUS 430 steel interconnect, J. Alloys Compd. 782 (2019) 100–109, https://doi.org/10.1016/j.jallcom.2018.12.174.
[41] S. Hu, W. Li, W. Li, N. Zhang, H. Qi, H. Finklea, X. Liu, A study on the electrophoretic deposition of gadolinium doped ceria on polypyrrole coated yttrium stabilized zirconia, J. Colloid Interface Sci. 555 (2019) 115–123, https://doi.org/10.1016/j.jcis.2019.07.094.